Robustifying dynamic positioning of crane vessels for heavy lifting operation

Ye, Jun; Roy, Spandan; Godjevac, Milinko; Reppa, Vasso; Baldi, Simone

DOI
10.1109/JAS.2021.1003913

Publication date
2021

Document Version
Final published version

Published in
IEEE/CAA Journal of Automatica Sinica

Robustifying Dynamic Positioning of Crane Vessels for Heavy Lifting Operation

Jun Ye, Spandan Roy, Milinko Godjevac, Vasso Reppa, *Member, IEEE*, and Simone Baldi, *Senior Member, IEEE*

***Abstract*—Construction crane vessels make use of dynamic positioning (DP) systems during the installation and removal of offshore structures to maintain the vessel's position. Studies have reported cases of instability of DP systems during offshore operation caused by uncertainties, such as mooring forces. DP "robustification" for heavy lift operations, i.e., handling such uncertainties systematically and with stability guarantees, is a long-standing challenge in DP design. A new DP method, composed by an observer and a controller, is proposed to address this challenge, with stability guarantees in the presence of uncertainties. We test the proposed method on an integrated cranevessel simulation environment, where the integration of several subsystems (winch dynamics, crane forces, thruster dynamics, fuel injection system etc.) allow a realistic validation under a wide set of uncertainties.**

***Index Terms*—Construction crane vessels, dynamic positioning system, offshore, robust control, uncertainty.**

I. Introduction

With the shortage of onshore energy sources, the need for energy is more and more satisfied by offshore wind turbines and offshore oil fields. These structures are transported/installed offshore by construction crane vessels. During offshore heavy lifting operations, the vessel needs to maintain its desired position via the so-called dynamic positioning (DP) system [1]. For a DP system to be effective, it is required to counteract the effect of external environmental forces such as wind and waves [2]–[5]. While attempting the positioning task, a DP system is subjected to a wide variety of uncertainty [6], such as the crane load [7]. For construction vessels such as dredgers, heavy-lift vessels, and pipe-laying vessels, additional uncertainties arise: in particular, uncertainties from unmodelled dynamics of the propulsion system and unmodelled forces become crucial during offshore heavy lift operation (see Fig. 1). Unmodelled dynamics of the propulsion system affect the precision of the DP system, since the propulsion system of a vessel cannot provide a fast response against disturbances induced by waves or measurement noises [3]; also, studies have shown that unmodelled forces propagating through the crane wires during heavy lifting operation (such uncertainties are commonly referred to as mooring forces) can cause unstable oscillatory behavior of the DP system [8], [9]. These uncertain scenarios bring challenges in the design of DP systems, which are of high interest due to the hazard during offshore heavy lifting operation.

In view of these challenges, research has focused on designing DP systems for offshore cranes in the presence of uncertainties [10]–[18]. Some works [10]–[12] mostly concentrated on the uncertainties in crane and load, neglecting uncertainties in vessel dynamics. Other works [13]–[18] studied structural uncertainties (e.g., mooring, damping forces) during offshore construction, neglecting the effect of disturbances and slow propulsion dynamics on DP performance. To address all uncertainty aspects in a comprehensive way, one should augment the DP system with an *observer* , whose task is to filter out disturbances in position/velocity measurements [1], [3], [19]. The design of such observers requires the accurate structural knowledge of the vessel dynamics and it is thus sensitive to unmodelled dynamics, as shown in [20]. It is worth remarking that literature provides observer designs such as high gain observer [21], extended state observer [22], and so on. However, the fast estimation response which is typically sought via these observers may not be suitable for real DP operation, mainly due to the fact that the thrusters and propellers of heavy-lift vessels cannot handle fast control command owing to their sheer sizes and their non-ideal behavior. There is no guarantee in general that the signals filtered by the observer will make the DP system operate in a stable way under such practical non-ideal effects [23]. Furthermore, recent studies on the control of offshore cranes focus on the vertical plane of the crane-load system, and neglected the impact from the sway disturbances and thruster delay [24]. The augmentation of a DP system with an observer results in a composite design. To the best of the authors' knowledge, composite DP designs

Manuscript received October 7, 2020; revised November 15, 2020; accepted December 16, 2020. This work was supported by the Program of China Scholarship Council (CSC) (20167720003), the Special Guiding Funds Double First-Class (3307012001A), and the Natural Science Foundation of China (62073074). Recommended by Associate Editor Zhanshan Wang. *(Corresponding author: Simone Baldi.)*

Citation: J. Ye, S. Roy, M. Godjevac, V. Reppa, and S. Baldi, "Robustifying dynamic positioning of crane vessels for heavy lifting operation," *IEEE/CAA J. Autom. Sinica*, vol. 8, no. 4, pp. 753–765, Apr. 2021.

J. Ye and V. Reppa are with the Department of Maritime and Transport Technology, Delft University of Technology, Delft 2628 CD, The Netherlands (e-mail: j.ye-1@tudelft.nl; v.reppa@tudelft.nl).

S. Roy is with the Robotics Research Center, International Institute of Information Technology Hyderabad, Hyderabad-500032, India (e-mail: spandan.roy@iiit.ac.in).

M. Godjevac is with the Future Proof Shipping, Delft 3013 AL, The Netherlands (e-mail: milinko.godjevac@gmail.com).

S. Baldi is with the School of Mathematics and School of Cyber Science and Engineering, Southeast University, Nanjing 210096, China, and guest with the Delft Center for System and Control, Delft University of Technology, Delft 2600 AA, The Netherlands (e-mail: s.baldi@tudelft.nl).

Color versions of one or more of the figures in this paper are available online at http://ieeexplore.ieee.org.

Digital Object Identifier 10.1109/JAS.2021.1003913

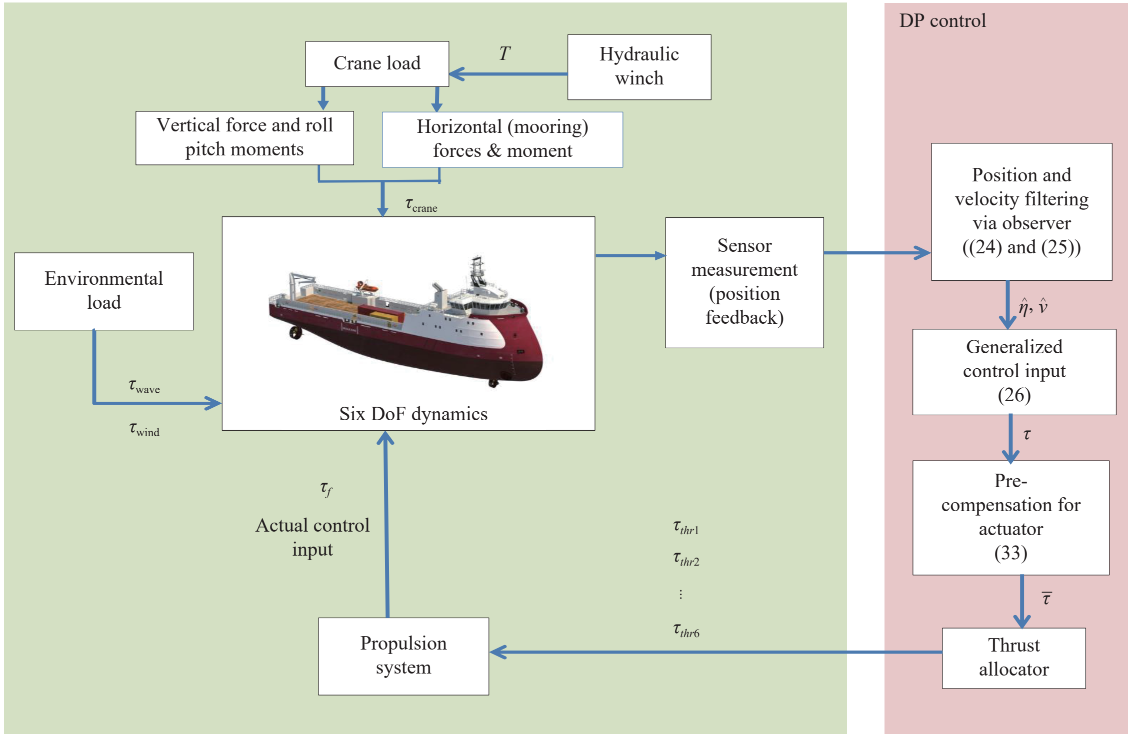

Fig. 1. Overall process plant model for the construction crane vessel. Unmodelled dynamics of the propulsion system affect the DP precision. Also, during offshore heavy lifting operation, instability of DP systems has been reported due to large mooring forces, which is the horizontal component of $\boldsymbol{\tau}_{\text{crane}}$.

without requiring *accurate structural knowledge* of vessel dynamics and with *stability guarantees* in the presence of uncertainty and unmodelled propulsion dynamics are missing in the literature.

To address this long-standing challenge, we treat mooring and hydrodynamics terms as the summation of a nominal part (which is known) and a perturbed part (which is unknown but bounded). The bounds of uncertainties do not require structural knowledge of the unknown dynamic terms, and can be used for robust control (worst-case) design. Meanwhile, the effect of the observer error (filtering) is proven to be bounded via robust stability analysis. The effectiveness of the proposed composite design is verified under the influence of various uncertainties via a realistic six DoFs simulation model, based on the S-175 model from MSS toolbox [25] with vessel dynamics generated by WAMIT, and augmented with a DP system and a hydraulic crane. Preliminary work by the authors on robust DP for heavy lift vessels was done in [26]: however, in [26] the presence of unmodelled propulsion dynamics is neglected. A point of interest of this study is to show that neglecting propulsion dynamics (engine dynamics, thruster dynamics, etc.) is not acceptable as it can lead to unstable DP behavior.

Summarizing, the innovations of this work are:

a) A detailed physical modelling for heavy lifting operations, where the integration of several subsystems allows to realistically simulate the effect of uncertainties;

b) A composite observer and controller solution to DP for offshore heavy lifting operations which, without requiring accurate structural knowledge of the vessel, can be proven stable even in the worst-case uncertainty settings (robust design). The proposed composite design comprises an artificial delay based method to tackle the unmodelled propulsion dynamics without priori knowledge.

c) Key performance indicators (KPIs) to guide the design while considering worst-case uncertainty and worst-case performance.

The paper is organized as follows: Section II models the physics of heavy lifting; Section III proposes the control strategy while Section IV analyzes its stability; simulation results are in Section V, with conclusions in Section VI.

The following notations will be used: $\lambda_{\min}(\bullet)$ and $\|\bullet\|$ represent minimum eigenvalue and Euclidean norm of $(\bullet)$ respectively; $\mathbf{I}$ denotes identity matrix with appropriate dimension; the trigonometric functions $\sin(\bullet)$, $\cos(\bullet)$, and $\tan(\bullet)$ are abbreviated as $s_\bullet$, $c_\bullet$, and $t_\bullet$; a vector $\mathbf{x} \in L_\infty$ implies that $\mathbf{x}$ is bounded in the infinity norm (cf. [27, Ch. 3]).

II. Control Objective

Because it was reported that instability in DP systems occurs during heavy-lift operation due to large mooring forces, it is crucial to model realistic dynamics. A realistic model that can describe realistic dynamics along six DoFs is commonly referred to in literature as a *process plant model* [28]: the process plant model in this work is based on the S-175 model from MSS toolbox [25], with vessel dynamics generated from WAMIT [29] and integrated with DP system and hydraulic crane. A schematic of the overall model is shown in Fig. 1. The process plant model allows to test a wide range of uncertain dynamical scenario, by including vessel dynamics, environmental loads, hydraulic crane, position controller, thrust allocator, diesel engines and thrusters. The various modules of the simulation model are individually detailed hereafter, and the simulation variables and parameters are collected in Table I.

TABLE I
SYSTEM PARAMETERS AND VARIABLES

Variables	Definitions
$\boldsymbol{\eta}_f$	The position and rotation angle of the vessel in NED
$\mathbf{J}(\phi,\theta,\psi)$	Rotation matrix from body-fixed to NED
$\boldsymbol{\nu}_f$	Body-fixed vessel velocity
$\boldsymbol{\nu}_c$	Body-fixed current velocity
$\boldsymbol{\nu}_{fr}$	Body-fixed relative velocity of the vessel w.r.t the current
$\boldsymbol{\tau}_f$	Thrust force
τ_{thri}	Thrust force of i-th thruster (scalar)
$\boldsymbol{\tau}_{thri}$	Forces and moments induced by i-th thruster (vector)
τ_{crane}	Crane induced forces and moments in surge, sway, heave, pitch, roll, and yaw
$\mathbf{G}(\boldsymbol{\eta}_f)$	Hydrostatic restoring force
$\bar{\mathbf{d}}_s$	External loads from wind and wave
τ_{wind}	Wind induced forces and moments
τ_{wave}	Wave induced forces and moments
F_{hoist}	Tension in the crane wires (scalar)
$\boldsymbol{F}$	Time-varying mooring stiffness in surge, sway, and yaw
T	Output torque of hydraulic motor
Q	Inlet flow rate
M_b	Output torque of diesel engine
M_p	Propeller output torque
n_p	Propeller's rate of revolution
$\boldsymbol{\tau}$	Control input
Parameters	
$\mathbf{M}_{RB}$	Rigid body mass matrix of the vessel in 6 DoFs
$\mathbf{M}_A$	Added mass matrix of the vessel in 6 DoFs
$\mathbf{D}_s$	Hydraulic damping matrix of the vessel in 6 DoFs
$\mathbf{C}(\boldsymbol{\nu}_{fr})$	Coriolis term in 6 DoFs
$\mathbf{B}_{ta}$	Thrust allocation matrix

A. Vessel Dynamics

Two coordinate systems are used to describe motion: body-fixed coordinate system and north-east-down (NED) coordinate system. For the body-fixed coordinate system, the center of origin is fixed on the vessel, with x-axis positive to the front of the vessel, y-axis positive to the right of the vessel, and z-axis positive downwards. For the NED coordinate system, the origin is fixed on the earth surface, with x-axis pointing the north, y-axis pointing to the east, and z-axis pointing downwards. The resulting dynamics of motion describe the six DoFs of the vessel: we follow the approach in [29, Eq. 8.5] under the assumptions of low velocity and acceleration and of irrotational and constant ocean currents:

$$\dot{\boldsymbol{\eta}}_f = \mathbf{J}'(\phi,\theta,\psi)\boldsymbol{\nu}_f \tag{1}$$

$$\begin{aligned}(\mathbf{M}_{RB}+\mathbf{M}_A)\dot{\boldsymbol{\nu}}_{fr} = &-(\mathbf{C}(\boldsymbol{\nu}_{fr})-\mathbf{D}_s(\boldsymbol{\nu}_{fr}))\boldsymbol{\nu}_{fr}-\boldsymbol{\tau}_{\text{crane}}\\ &-\mathbf{g}_0-\mathbf{G}(\boldsymbol{\eta}_f)+\bar{\boldsymbol{d}}_s+\boldsymbol{\tau}_f\end{aligned} \tag{2}$$

$$\bar{\boldsymbol{d}}_s = \boldsymbol{\tau}_{\text{wind}}+\boldsymbol{\tau}_{\text{wave}}$$

where $\boldsymbol{\eta}_f = [x\, y\, z\, \phi\, \theta\, \psi]^T$ is the vessel position in NED coordinate system, in which (x,y,ψ) denote the surge, sway and yaw angle of the vessel, and (z,ϕ,θ) denote the heave position, roll and pitch angles of the vessel; $\boldsymbol{\nu}_{fr} = \boldsymbol{\nu}_f-\boldsymbol{\nu}_c$ denote the relative velocity of the vessel with respect to the current velocity $\boldsymbol{\nu}_c = [u_c, v_c, 0, 0, 0, 0]^T$, where $\boldsymbol{\nu}_f = [u, v, w, p, q, r]^T$ is the vessel velocity (all in body-fixed coordinate system); $\mathbf{J}'(\phi,\theta,\psi)$ is the body-to-NED rotation matrix

$$\mathbf{J}'(\phi,\theta,\psi) = \begin{bmatrix} \mathbf{R}_b^n & \mathbf{0}^{3\times3} \\ \mathbf{0}^{3\times3} & \mathbf{T}_b^n \end{bmatrix} \tag{3}$$

where

$$\mathbf{R}_b^n = \begin{bmatrix} c_\psi c_\theta & -s_\psi c_\theta + c_\psi s_\theta s_\phi & s_\psi c_\phi s_\theta \\ s_\psi c_\theta & c_\psi c_\phi + s_\phi s_\theta s_\psi & -c_\psi s_\phi + s_\theta s_\psi c_\phi \\ -s_\theta & c_\theta s_\phi & c_\theta c_\phi \end{bmatrix} \tag{4}$$

$$\mathbf{T}_b^n = \begin{bmatrix} 1 & s_\phi t_\theta & c_\phi t_\theta \\ 0 & c_\phi & -s_\phi \\ 0 & \frac{s_\phi}{c_\theta} & \frac{c_\phi}{c_\theta} \end{bmatrix}. \tag{5}$$

The external disturbance $\bar{\mathbf{d}}_s$ comprises of the external loads from wind ($\boldsymbol{\tau}_{\text{wind}}$) and wave ($\boldsymbol{\tau}_{\text{wave}}$); $\boldsymbol{\tau}_{\text{crane}}$ are the crane forces and moments in six DoFs, which also contain the three DoFs (in surge, sway, and yaw) mooring forces and moment; $\boldsymbol{\tau}_f = [\tau_x, \tau_y, 0, 0, 0, \tau_\psi]$ is the thrust force in six DoFs; $\mathbf{G}(\boldsymbol{\eta}_f)$ and $\mathbf{g}_0 = [0\; 0\; -Mg\; 0\; 0\; 0]^T$ are the restoring and gravity forces, where M is the mass of the vessel and g is the gravitational acceleration.

The terms $\mathbf{M}_{RB}, \mathbf{M}_A, \mathbf{C}(\boldsymbol{\nu}_{fr})$, and $\mathbf{D}_s$ denote the rigid body mass matrix, added mass matrix, Coriolis terms, and hydrodynamic damping terms, respectively; consistently with [29], the inertia matrix $\mathbf{M}_{RB} \in \mathbb{R}^{6\times6}$ is defined as

$$\mathbf{M}_{RB} = \begin{bmatrix} m\mathbf{I}_{3\times3} & -m\mathbf{S}(\mathbf{r}_g^b) \\ m\mathbf{S}(\mathbf{r}_g^b) & \mathbf{J}_v \end{bmatrix} \tag{6}$$

where m is the weight of the vessel, $\mathbf{J}_v$ is the inertia moment matrix in roll pitch and yaw, $\mathbf{r}_g^b$ is the vector from Center of Origin to Center of Gravity expressed in body frame, and the cross-product is defined as $\mathbf{a}\times\mathbf{b} = \mathbf{S}(\mathbf{a})\mathbf{b}$.

For a vessel which is symmetric on port-starboard, the added mass and added inertia matrix can be expressed as

$$\mathbf{M}_A = \begin{bmatrix} m_{11} & 0 & m_{13} & 0 & m_{15} & 0 \\ 0 & m_{22} & 0 & m_{24} & 0 & m_{26} \\ m_{31} & 0 & m_{33} & 0 & m_{35} & 0 \\ 0 & m_{42} & 0 & m_{44} & 0 & m_{46} \\ m_{51} & 0 & m_{53} & 0 & m_{55} & 0 \\ 0 & m_{62} & 0 & m_{64} & 0 & m_{66} \end{bmatrix} \tag{7}$$

where m_{ij} can be expressed as: $m_{ij} = \rho_w \oint_S \varphi_i \frac{\partial\varphi_j}{\partial n} dS$, where ρ_w is the density of sea water, S is the wetted ship area, φ_i is the flow potential when the vessel is moving in ith direction.

When the roll and pitch angle is small, the restoring force

$\mathbf{G}(\boldsymbol{\eta}_f)$ can be expressed as

$$\mathbf{G}(\boldsymbol{\eta}_f) = \begin{bmatrix} 0 \\ 0 \\ \rho_w g A_{wp} z \\ \rho_w g \nabla \overline{GM}_T \phi \\ \rho_w g \nabla \overline{GM}_L \theta \\ 0 \end{bmatrix} \tag{8}$$

where A_{wp} is the water plane area of the vessel, and it is assumed that A_{wp} stays constant for small heave movement; ∇ is the nominal displaced water volume; $\overline{GM}_T$ and $\overline{GM}_L$ denote transverse metacentric height and longitudinal metacentric height, respectively. The terms $\mathbf{C}$ and $\mathbf{D}_s$ are considered according to [29, Sect. 7.3.1].

B. Environmental Loads

The environmental loads can be seen as the combination of wind load and wave load. Wind load is related to the surface of the vessel above the waterline, wind velocity and attack angle of the wind, causing additional air pressure to the surface of the vessel. For a vessel in DP control mode with zero speed over ground, the wind load can be defined as

$$\boldsymbol{\tau}_{\text{wind}} = \frac{1}{2}\rho_a V_w^2 \begin{bmatrix} C_X(\gamma_w) A_{Fw} \\ C_Y(\gamma_w) A_{Lw} \\ C_Z(\gamma_w) A_{Fw} \\ C_K(\gamma_w) A_{Lw} H_{Lw} \\ C_M(\gamma_w) A_{Fw} H_{Fw} \\ C_N(\gamma_w) A_{Lw} L_{oa} \end{bmatrix} \tag{9}$$

where ρ_a is air density, V_w is wind speed, modeled as a combination of slow-varying wind and wind gust; C_X, C_Y, C_Z, C_K, C_M, and C_N are nondimensional coefficients related to the angle of attack, and can be caculated from [29, Eq. 8.30–8.36]; A_{Fw} and A_{Lw} are the frontal and lateral project areas above the waterline, while H_{Fw} and H_{Lw} are the centroids of the two areas, and γ_w is the angle of attack of the wind. The wind angle is considered to be slowly varying around the mean wind angle. The wave load $\boldsymbol{\tau}_{\text{wave}}$ is modeled as a the sum of a first-order wave (zero mean oscillation load) and a second order wave (mean wave drift load without oscillatory component) (cf. [29, Eq. 8.88–8.89] for their detailed structure).

C. Hydraulic Crane

The crane model consists of a hydraulic crane and the crane wires. Assuming no slack, the crane wires are modelled as a spring and a damper [30]

$$F_{\text{hoist}} = k_w(l_w(t) - l_{\text{ini}}(t)) + D_w \frac{d}{dt}(l_w(t) - l_{\text{ini}}(t)) \tag{10}$$

where $F_{\text{hoist}} = \sqrt{\mathbf{F}^2_{\text{hoist}_x} + \mathbf{F}^2_{\text{hoist}_y} + \mathbf{F}^2_{\text{hoist}_z}}$ is the norm of the tension in the crane wires, k_w is the stiffness of the crane wires, D_w is the damping term of the wires, l_w and l_{ini} are the instantaneous length and initial length of the crane wires, respectively. During the simulation, l_{ini} is changing to adjust the output torque from the hydraulic motor.

The crane winch is actuated by a PI-controlled hydraulic motor, typically designed by the crane manufacturer. The output torque T of the hydraulic motor is [31]

$$T = \frac{\eta_{\text{hyd}} Q \Delta p}{2\pi}, \quad F_{\text{hoist}} = \frac{T}{r} \tag{11}$$

$$Q = K_{hp}\delta T + \int K_{hi}\delta T\, dt \tag{12}$$

where Q is the inlet flow rate per revolution; Δp is the pressure difference between the inlet flow and the outlet flow, η_{hyd} is the efficiency of the motor; r is the radius of the drum that the cable is wound on, where δT is the difference between the user-defined required torque and the actual torque. The PI controller has been tuned according to reaction curve based methods as in [32, Sect. 6.5] in such a way that the time constant of the output torque is around 1 s.

D. Propulsion System

To properly capture the dynamics of the propulsion system, we use a mean-value first principle modelling for engine-propeller interaction (cf. [33], [34] for details). The diesel engine is modeled as a four-stroke engine with six cylinders

$$M_b = \frac{6\eta_e m_f k_{\text{LHV}} n_{\text{eng}}}{2\pi n_{\text{eng}}} \tag{13}$$

where M_b is the output torque; η_e is the efficiency, m_f is the fuel injection in gramme; k_{LHV} is the lower heating value (a.k.a fuel energy/mass ratio), and n_{eng} is the engine speed in rotation per second. The thrust force for each thruster i is

$$\begin{aligned} \tau_{thri} &= \rho_w n^2 D^4_{\text{prop}} K_t \\ &= \rho_w n_p^2 D^4_{\text{prop}} (K_{ta} \frac{V_A}{n_p D_{\text{prop}}} + K_{tb}) \end{aligned} \tag{14}$$

where ρ_w is the water density; n_p is the rate of revolution; D_{prop} is the diameter of the propeller; K_{ta} and K_{tb} are two constant parameters; V_A is the arriving water velocity.

Similarly, the propeller torque is

$$\begin{aligned} M_p &= \rho_w n_p^2 D^5_{\text{prop}} K_q \\ &= \rho_w n_p^2 D^5_{\text{prop}} (K_{qa} \frac{V_A}{n_p D_{\text{prop}}} + K_{qb}). \end{aligned} \tag{15}$$

A shaft is connected between the diesel engine and the propeller with a gearbox. The rate of revolution of the propeller can be described as

$$n_p = \frac{n_e}{i_{gb}} = \int \frac{M_b \eta_{\text{trm}} i_{gb} - M_p}{2\pi I_{\text{tot}}} dt \tag{16}$$

where i_{gb} is the gearbox ratio, η_{trm} is the transmission efficiency, and I_{tot} is the total mass of inertia of the propulsion system. The overall thrust force on the vessel is computed as

$$\boldsymbol{\tau}_f = \sum \tau_{thri} \tag{17}$$

where the summation is to be intended as vector summation.

A thrust allocator is designed for the engine-thrust system

$$\begin{bmatrix} \tau_{thr1} \\ \tau_{thr2} \\ \vdots \\ \tau_{thr6} \end{bmatrix} = \mathbf{B}_{ta}\boldsymbol{\tau} \tag{18}$$

where $\mathbf{B}_{ta}$ is designed based on the knowledge of the positions of the thrusters [30].

III. Controller Design

While the performance of a DP system is better validated on realistic six DoFs as in the process plant model (1) and (2), the DP design is conventionally performed on a three DoFs *control plant model* [28]. The three DoFs arise from the $[x, y, \psi]$ coordinates (also known as surge, sway, and yaw) [29, Sect. 7.3.1], resulting in

$$\dot{\boldsymbol{\eta}} = \mathbf{J}(\psi)\boldsymbol{\nu} \tag{19}$$

$$\mathbf{M}\dot{\boldsymbol{\nu}} = -\mathbf{D}\boldsymbol{\nu} - \mathbf{F}\boldsymbol{\eta} + \boldsymbol{\tau} + \mathbf{d}_s \tag{20}$$

$$\mathbf{J}(\psi) = \begin{bmatrix} c_\psi & -s_\psi & 0 \\ s_\psi & c_\psi & 0 \\ 0 & 0 & 1 \end{bmatrix} \tag{21}$$

where $\boldsymbol{\eta} = [x, y, \psi]^T$ comprises of north position, east position and heading angle; $\boldsymbol{\nu} = [u, v, r]^T$ is the vessel velocity/angular velocity in body-fixed coordinate system; $\boldsymbol{\tau} = [\tau_x, \tau_y, \tau_\psi]$; $\mathbf{M} \in \mathbb{R}^{3\times3}$ is the combination of rigid body mass/inertia matrix and added mass matrix in three DoFs which are obtained by considering only the $[x, y, \psi]$ components of the six DoFs matrix $\bar{\mathbf{M}} = \mathbf{M}_{RB} + \mathbf{M}_A$ in (2), and is a positive definite matrix [29]; similarly, $\mathbf{D} \in \mathbb{R}^{3\times3}$ is the three DoFs version of $\mathbf{D}_s$; $\mathbf{d}_s$ is the combination of external loads on $[x, y, \psi]$ coordinates; $\mathbf{F}\boldsymbol{\eta}$ denotes the mooring force with $\mathbf{F} \in \mathbb{R}^{3\times3}$ being the positive definite spring coefficient matrix arising from the linearization of crane force in surge, sway, and yaw (cf. [30] for the detailed steps of linearization). Without loss of generality, we consider $[0, 0, 0]^T$ to be the desired position of the vessel.

Remark 1 (Control Plant Model vs. Process Plant Model): Reducing a process plant model to a control plant model, i.e., from 6 to 3 DoFs, introduces unmodelled dynamics. Unmodelled dynamics in (20) as compared to (2) are

1) The terms $\boldsymbol{C}, \boldsymbol{G}$, and $\boldsymbol{g}_0$;
2) The thruster dynamics;
3) The damping components of the crane wires.

Therefore, the simulations using the six DoF process plant will allow to test the performance of the proposed design in representative dynamical uncertain scenarios. A DP system must be designed so as to tackle all such uncertainties.

In the following we will describe how uncertainty is included in the three DoF control plant model (20).

A. Uncertainty Setting

Henceforth, for compactness, $\mathbf{J}(\psi)$ will be represented as $\mathbf{J}$, and the system dynamics (19) and (20) is represented as

$$\dot{\boldsymbol{\eta}} = \mathbf{J}\boldsymbol{\nu} \tag{22}$$

$$\dot{\boldsymbol{\nu}} = -\mathbf{A}_1\boldsymbol{\eta} - \mathbf{A}_2\boldsymbol{\nu} + \mathbf{M}^{-1}\boldsymbol{\tau} + \mathbf{d} \tag{23}$$

where $\mathbf{A}_1 \triangleq \mathbf{M}^{-1}\mathbf{F}, \mathbf{A}_2 \triangleq \mathbf{M}^{-1}\mathbf{D}$, $\mathbf{d} \triangleq \mathbf{M}^{-1}\mathbf{d}_s$ and $\mathbf{M}$ is positive definite matrix [20]. Note that in crane vessels the exact values of the positive definite matrices $\mathbf{A}_1$ and $\mathbf{A}_2$ is subject to uncertainty. The following assumption highlights the nature of uncertainties considered in this work for dynamics (20):

Assumption 1 (Uncertainty): $\boldsymbol{A}_i$'s can be decomposed into two positive definite matrices $\hat{\boldsymbol{A}}_i$ (nominal part) and $\tilde{\boldsymbol{A}}_i$ (unknown perturbation), i.e., $\boldsymbol{A}_i(t) = \hat{\boldsymbol{A}}_i + \tilde{\boldsymbol{A}}_i(t)$. Quantities available for control designs are: the maximum perturbation ranges $\Delta\boldsymbol{A}_i$ (such that $\|\Delta\boldsymbol{A}_i\| \geq \|\tilde{\boldsymbol{A}}_i(t)\|\ \forall t$); the mass matrix $\mathbf{M}$; the upper bound $\Delta\boldsymbol{d}$ on the external disturbances (such that $\|\Delta\boldsymbol{d}\| \geq \|\boldsymbol{d}(t)\|\ \forall t$).

Remark 2 (Robustification Philosophy): The perturbation ranges $\Delta\boldsymbol{A}_i$ define the worst-case uncertainty in mooring and hydrodynamic damping forces. The upper bound $\Delta\boldsymbol{d}$ defines the worst-case environmental conditions. The knowledge of these terms is required if one aims at proving stability of the DP system in the worst-case uncertainty settings. Differently from mooring and hydrodynamic damping terms, the mass $\mathbf{M}$ of a vessel is typically known with little uncertainty. In fact, uncertainty in mass matrix arise from movements in water with high acceleration or deceleration (added mass terms), which are negligible during DP operation [29]. Such values of the vessel can be obtained from the data provided by contractors.

B. Observer-Based Robust Control

The composite DP design can now be proposed

$$\dot{\hat{\boldsymbol{\eta}}} = -\mathbf{K}\hat{\boldsymbol{\eta}} + \mathbf{K}_1\tilde{\boldsymbol{\eta}} + \mathbf{J}\hat{\boldsymbol{\nu}} \tag{24}$$

$$\dot{\hat{\boldsymbol{\nu}}} = -\hat{\mathbf{A}}_1\hat{\boldsymbol{\eta}} - \hat{\mathbf{A}}_2\hat{\boldsymbol{\nu}} + \mathbf{M}^{-1}\boldsymbol{\tau} + \mathbf{K}_2\tilde{\boldsymbol{\eta}} \tag{25}$$

$$\boldsymbol{\tau} = \mathbf{M}\left(\hat{\mathbf{A}}_1\hat{\boldsymbol{\eta}} + \hat{\mathbf{A}}_2\hat{\boldsymbol{\nu}} - \mathbf{K}_2\tilde{\boldsymbol{\eta}} - \mathbf{J}^T\hat{\boldsymbol{\eta}} - (\rho + \rho_1)\hat{\boldsymbol{\nu}}\right) \tag{26}$$

whose stability analysis will be given in Section IV. It consists of a composite design of robust controller and observer: observers for positions and velocities via (24) and (25) helps to filter out disturbances and ease the thrusters' action (cf. (18)).

In order to handle the worst-case uncertainty settings, the observer and control gains $\mathbf{H}, \mathbf{K}, \mathbf{K}_1, \mathbf{K}_2, \rho_1$, and ρ should be properly designed. The design of such gains is proposed as

$$\lambda_{\min}(\mathbf{K}_1) > \|\frac{1}{2\beta_2}(\Delta\mathbf{A}_1 + \mathbf{K}_2)^T\mathbf{H}_2^{-1}(\Delta\mathbf{A}_1 + \mathbf{K}_2)\| \tag{27}$$

$$\lambda_{\min}(\mathbf{K}) > \|\frac{1}{2\beta_3}(\Delta\mathbf{A}_1 + \mathbf{K}_2)^T\mathbf{H}_3^{-1}(\Delta\mathbf{A}_1 + \mathbf{K}_2)\| \tag{28}$$

$$\rho > \|(\frac{1}{2\beta_1})\Delta\mathbf{A}_2^T\mathbf{H}_1^{-1}\Delta\mathbf{A}_2\| + \|\Delta\mathbf{d}\| \tag{29}$$

$$\rho_1(t) = \alpha\int_{t-h}^{t}\|(\mathbf{K}_1 + \mathbf{K})\|\|\hat{\boldsymbol{\eta}}(\zeta)\|\|\boldsymbol{\eta}(\zeta) - \hat{\boldsymbol{\eta}}(\zeta)\|\mathrm{d}\zeta \tag{30}$$

$$\mathbf{K}_2(t) = -\hat{\mathbf{A}}_1 + \mathbf{J}^T(t) \tag{31}$$

where $\alpha > 1$; β_i and $\mathbf{H}_i$ $i = 1, 2, 3$ denote positive scalars and positive definite matrices that must satisfy

$$\|(\frac{1}{2})(\beta_1\mathbf{H}_1 + \beta_2\mathbf{H}_2 + \beta_3\mathbf{H}_3)\| < \lambda_{\min}(\hat{\mathbf{A}}_2). \tag{32}$$

In (30), $h > 0$ is an artificially induced delay (i.e., use of past ρ_1) and its choice is discussed in the subsequent section.

Remark 3 (Selection of Gains): According to Assumption 1, $\hat{\mathbf{A}}_2$ is defined based on the nominal knowledge of $\mathbf{A}_2$. Therefore, condition (32) provides a selection criterion for β_i and $\mathbf{H}_i$, which in turn guides to select the other gains $\mathbf{K}_1, \mathbf{K}, \rho$, and ρ_1 from (27), (28), (29), and (30), respectively. Note that $\mathbf{J}$ is an orthogonal matrix with $\|\mathbf{J}(\psi)\| = 1\ \forall\psi$; thus, one can easily compute the upper bounds of the right hand sides in (27) and (28) when designing $\mathbf{K}_1$ and $\mathbf{K}$.

C. Precompensation for Unmodelled Thruster Dynamics

The dynamics of the thrusters include a limitation of propulsion rate and a time delay which can be modelled approximately as a low pass filter. Such low pass filter introduces unmodelled dynamics which, if left unattended, might lead to unstable closed-loop behaviour. In view of such scenario, inspired from [35], we employ an artificial delay based precompensation method as

$$\bar{\tau}_i(t) = N_i\tau_i(t) - \bar{N}_i\tau_i(t-h),\ i = 1,2,3 \tag{33}$$

where $\boldsymbol{\tau} = \{\tau_1, \tau_2, \tau_3\}$; $\bar{\tau}_i$ denotes the input to the thrust allocator; N_i and $\bar{N}_i$ are two positive scalars, $\tau_i(t-h)$ requires to artificially use of a past control input of previous sampling time (being $h > 0$ the so-called artificial time delay).

To design N_i and $\bar{N}_i$, one notes that boundedness of $\boldsymbol{\tau}(t)$ is established in (56) following [35]. Therefore, given an h, one needs to design N_i and $\bar{N}_i$ such that boundedness of $\bar{\tau}_i$ can be established from boundedness of $\boldsymbol{\tau}(t)$. As the sampling time of DP system is of typically small (order of hundredth of a second), $\tau_i(t-h)$ can be approximated via Padé approximation

$$\bar{\tau}_i(s) = N_i\tau_i(s) - \bar{N}_i\frac{-\frac{h}{2}s+1}{\frac{h}{2}s+1}\boldsymbol{\tau}(s)$$
$$\Rightarrow \frac{\bar{\tau}_i(s)}{\tau_i(s)} = \frac{(N_i+\bar{N}_i)hs + 2(N_i-\bar{N}_i)}{hs+2} \tag{34}$$

where s is the Laplace operator. One can verify that any $\bar{N}_i$ satisfying $0 < \bar{N}_i < N_i$ leads to minimum phase dynamics for (34), i.e., the precompensation (33) will not invalidate the closed-loop stability of the subsequent Section IV.

Remark 4 (Available Measurements): The proposed observer-based robust controller requires position measurements but no velocity measurements. Removing noisy velocity feedback is especially relevant in surface operation [36], when one can rely on GNSS systems (e.g., GPS/GLONASS and Galileo [37]), or relative positioning systems based on lasers and cameras. On the other hand, velocity feedback becomes beneficial in environments where the aforementioned measurements are not possible (e.g., underwater) [38].

IV. Stability/Performance of the Proposed DP

We first give the stability analysis of the proposed controller and consequently, we highlight some key performance indicators to drive the selection of the design parameters.

Definition 1 (Globally Uniformly Ultimately Bounded Stability [39]): System (22) and (23) is globally uniformly ultimately bounded if there exists a convex and compact set Υ such that for every initial condition $(\boldsymbol{\eta}(0), \boldsymbol{\nu}(0))$, there exists a finite $T(\boldsymbol{\eta}(0), \boldsymbol{\nu}(0))$ such that $(\boldsymbol{\eta}(t), \boldsymbol{\nu}(t)) \in \Upsilon$ for all $t \geq T$.

A. Main Stability Result

Theorem 1: Under Assumption 1, the system (22) and (23) employing the controller (24)–(26) remains uniformly ultimately bounded (UUB) if, for given $\beta_i > 0$ and $\mathbf{H}_i > \mathbf{0}$ $1 = 1,2,3$, the selection of the gains $\mathbf{K}, \mathbf{K}_1, \mathbf{K}_2, \hat{\mathbf{A}}_2, \rho$, and ρ_1 satisfy (27)–(32).

Proof: Let us define $\tilde{\boldsymbol{\eta}} \triangleq \boldsymbol{\eta} - \hat{\boldsymbol{\eta}}$ and $\tilde{\boldsymbol{\nu}} \triangleq \boldsymbol{\nu} - \hat{\boldsymbol{\nu}}$; where $\hat{\boldsymbol{\eta}}$ and $\hat{\boldsymbol{\nu}}$ are the observed (filtered) values of $\boldsymbol{\eta}$ and $\boldsymbol{\nu}$, respectively, and $\tilde{\boldsymbol{\eta}} \triangleq \boldsymbol{\eta} - \hat{\boldsymbol{\eta}}$, $\tilde{\boldsymbol{\nu}} \triangleq \boldsymbol{\nu} - \hat{\boldsymbol{\nu}}$. The closed-loop system stability is proved using the following Lyapunov function:

$$V(\boldsymbol{\xi}) = V_1(\tilde{\boldsymbol{\eta}}, \tilde{\boldsymbol{\nu}}) + V_2(\hat{\boldsymbol{\eta}}, \hat{\boldsymbol{\nu}}) \tag{35}$$

where $\boldsymbol{\xi} \triangleq [\tilde{\boldsymbol{\eta}}^T\ \tilde{\boldsymbol{\nu}}^T\ \hat{\boldsymbol{\eta}}^T\ \hat{\boldsymbol{\nu}}^T]^T$, $V_1 \triangleq (\frac{1}{2}\tilde{\boldsymbol{\eta}}^T\tilde{\boldsymbol{\eta}} + \frac{1}{2}\tilde{\boldsymbol{\nu}}^T\tilde{\boldsymbol{\nu}})$ and $V_2 \triangleq (\frac{1}{2}\hat{\boldsymbol{\eta}}^T\hat{\boldsymbol{\eta}} + \frac{1}{2}\hat{\boldsymbol{\nu}}^T\hat{\boldsymbol{\nu}})$. Using (22)–(25), the observer error dynamics are

$$\dot{\tilde{\boldsymbol{\eta}}} = \dot{\boldsymbol{\eta}} - \dot{\hat{\boldsymbol{\eta}}} = \mathbf{J}\tilde{\boldsymbol{\nu}} + \mathbf{K}\hat{\boldsymbol{\eta}} - \mathbf{K}_1\tilde{\boldsymbol{\eta}} \tag{36}$$

$$\begin{aligned}\dot{\tilde{\boldsymbol{\nu}}} = \dot{\boldsymbol{\nu}} - \dot{\hat{\boldsymbol{\nu}}} = &-\hat{\mathbf{A}}_1\tilde{\boldsymbol{\eta}} - \tilde{\mathbf{A}}_1(\tilde{\boldsymbol{\eta}} + \hat{\boldsymbol{\eta}}) - \mathbf{K}_2\hat{\boldsymbol{\eta}}\\ &- \hat{\mathbf{A}}_2\tilde{\boldsymbol{\nu}} - \tilde{\mathbf{A}}_2(\tilde{\boldsymbol{\nu}} + \hat{\boldsymbol{\nu}}) + \mathbf{d}.\end{aligned} \tag{37}$$

From (31) and (36)–(37), the following can be achieved:

$$\begin{aligned}\dot{V}_1 = &-\tilde{\boldsymbol{\eta}}^T\mathbf{K}_1\tilde{\boldsymbol{\eta}} - \tilde{\boldsymbol{\nu}}^T(\hat{\mathbf{A}}_2 + \tilde{\mathbf{A}}_2)\tilde{\boldsymbol{\nu}} + \tilde{\boldsymbol{\eta}}^T\mathbf{K}\hat{\boldsymbol{\eta}}\\ &- \tilde{\boldsymbol{\nu}}^T(\tilde{\mathbf{A}}_1 - \mathbf{K}_2)\hat{\boldsymbol{\eta}} - \tilde{\boldsymbol{\nu}}^T\tilde{\mathbf{A}}_2\hat{\boldsymbol{\nu}}\\ &- \tilde{\boldsymbol{\nu}}^T(\tilde{\mathbf{A}}_1 + \mathbf{K}_2)\hat{\boldsymbol{\eta}} + \tilde{\boldsymbol{\nu}}^T\mathbf{d}\\ \leq &-\tilde{\boldsymbol{\eta}}^T\mathbf{K}_1\tilde{\boldsymbol{\eta}} - \tilde{\boldsymbol{\nu}}^T\hat{\mathbf{A}}_2\tilde{\boldsymbol{\nu}} + \tilde{\boldsymbol{\eta}}^T\mathbf{K}\hat{\boldsymbol{\eta}} + \tilde{\boldsymbol{\nu}}^T\mathbf{d} - \tilde{\boldsymbol{\nu}}^T\tilde{\mathbf{A}}_2\hat{\boldsymbol{\nu}}\\ &- \tilde{\boldsymbol{\nu}}^T(\tilde{\mathbf{A}}_1 - \mathbf{K}_2)\hat{\boldsymbol{\eta}} - \tilde{\boldsymbol{\nu}}^T(\tilde{\mathbf{A}}_1 + \mathbf{K}_2)\hat{\boldsymbol{\eta}}\end{aligned} \tag{38}$$

where we have used the fact that $\tilde{\mathbf{A}}_2$ is positive definite from Assumption 1. Further, using (24)–(26), the following holds:

$$\begin{aligned}\dot{V}_2 &= \hat{\boldsymbol{\eta}}^T(-\mathbf{K}\hat{\boldsymbol{\eta}} + \mathbf{K}_1\tilde{\boldsymbol{\eta}} + \mathbf{J}\hat{\boldsymbol{\nu}}) + \hat{\boldsymbol{\nu}}^T(-(\rho+\rho_1)\hat{\boldsymbol{\nu}} - \mathbf{J}^T\hat{\boldsymbol{\eta}})\\ &= -\hat{\boldsymbol{\eta}}^T\mathbf{K}\hat{\boldsymbol{\eta}} - (\rho+\rho_1)\|\hat{\boldsymbol{\nu}}\|^2 + \hat{\boldsymbol{\eta}}^T\mathbf{K}_1\tilde{\boldsymbol{\eta}}.\end{aligned} \tag{39}$$

Given any scalar $\beta > 0$ and a positive definite matrix $\mathbf{H}$, the following holds for any two non-zero vectors $\mathbf{z}$ and $\mathbf{z}_1$ [40], [41]:

$$\pm 2\mathbf{z}^T\mathbf{z}_1 \leq \beta\mathbf{z}^T\mathbf{H}\mathbf{z} + (\frac{1}{\beta})\mathbf{z}_1^T\mathbf{H}^{-1}\mathbf{z}_1. \tag{40}$$

Applying (40) to the last three terms of (38) the following relations are obtained for $\beta_i > 0, \mathbf{H}_i > \mathbf{0}$ $i = 1,2,3$:

$$-\tilde{\boldsymbol{\nu}}^T\tilde{\mathbf{A}}_2\hat{\boldsymbol{\nu}} \leq (\frac{\beta_1}{2})\tilde{\boldsymbol{\nu}}^T\mathbf{H}_1\tilde{\boldsymbol{\nu}} + (\frac{1}{2\beta_1})\{\tilde{\mathbf{A}}_2\hat{\boldsymbol{\nu}}\}^T\mathbf{H}_1^{-1}\{\tilde{\mathbf{A}}_2\hat{\boldsymbol{\nu}}\} \tag{41}$$

$$\begin{aligned}-\tilde{\boldsymbol{\nu}}^T(\tilde{\mathbf{A}}_1 - \mathbf{K}_2)\hat{\boldsymbol{\eta}} \leq\ &(\frac{\beta_2}{2})\tilde{\boldsymbol{\nu}}^T\mathbf{H}_2\tilde{\boldsymbol{\nu}}\\ &+ (\frac{1}{2\beta_2})\hat{\boldsymbol{\eta}}^T(\tilde{\mathbf{A}}_1 - \mathbf{K}_2)^T\mathbf{H}_2^{-1}(\tilde{\mathbf{A}}_1 - \mathbf{K}_2)\hat{\boldsymbol{\eta}}\end{aligned} \tag{42}$$

$$\begin{aligned}-\tilde{\boldsymbol{\nu}}^T(\tilde{\mathbf{A}}_1 + \mathbf{K}_2)\hat{\boldsymbol{\eta}} \leq\ &(\frac{\beta_3}{2})\tilde{\boldsymbol{\nu}}^T\mathbf{H}_3\tilde{\boldsymbol{\nu}}\\ &+ (\frac{1}{2\beta_3})\hat{\boldsymbol{\eta}}^T(\tilde{\mathbf{A}}_1 + \mathbf{K}_2)^T\mathbf{H}_3^{-1}(\tilde{\mathbf{A}}_1 + \mathbf{K}_2)\hat{\boldsymbol{\eta}}.\end{aligned} \tag{43}$$

From the upper bound condition $\|\tilde{\mathbf{A}}_i\| \leq \|\Delta\mathbf{A}_i\|$ in Assumption 1, one can verify the following quadratic relations:

$$\{\tilde{\mathbf{A}}_2\hat{\boldsymbol{\nu}}\}^T\mathbf{H}_1^{-1}\{\tilde{\mathbf{A}}_2\hat{\boldsymbol{\nu}}\} \leq \{\Delta\mathbf{A}_2\hat{\boldsymbol{\nu}}\}^T\mathbf{H}_1^{-1}\{\Delta\mathbf{A}_2\hat{\boldsymbol{\nu}}\} \tag{44}$$

$$(\tilde{\mathbf{A}}_1 \pm \mathbf{K}_2)^T \mathbf{H}_j^{-1} (\tilde{\mathbf{A}}_1 \pm \mathbf{K}_2) \le (\Delta\mathbf{A}_1 + \mathbf{K}_2)^T \mathbf{H}_j^{-1} (\Delta\mathbf{A}_1 + \mathbf{K}_2),\ j = 1,2. \quad (45)$$

Using the above inequalities, the relation (41)–(43) are simplified to

$$-\tilde{\boldsymbol{\nu}}^T \tilde{\mathbf{A}}_2 \hat{\boldsymbol{\nu}} \le (\frac{\beta_1}{2}) \tilde{\boldsymbol{\nu}}^T \mathbf{H}_1 \tilde{\boldsymbol{\nu}} + (\frac{1}{2\beta_1}) \{\Delta\mathbf{A}_2 \hat{\boldsymbol{\nu}}\}^T \mathbf{H}_1^{-1} \{\Delta\mathbf{A}_2 \hat{\boldsymbol{\nu}}\} \quad (46)$$

$$-\tilde{\boldsymbol{\nu}}^T (\tilde{\mathbf{A}}_1 - \mathbf{K}_2) \tilde{\boldsymbol{\eta}} \le (\frac{\beta_2}{2}) \tilde{\boldsymbol{\nu}}^T \mathbf{H}_2 \tilde{\boldsymbol{\nu}} + (\frac{1}{2\beta_2}) \tilde{\boldsymbol{\eta}}^T (\Delta\mathbf{A}_1 + \mathbf{K}_2)^T \mathbf{H}_2^{-1} (\Delta\mathbf{A}_1 + \mathbf{K}_2) \tilde{\boldsymbol{\eta}} \quad (47)$$

$$-\tilde{\boldsymbol{\nu}}^T (\tilde{\mathbf{A}}_1 + \mathbf{K}_2) \hat{\boldsymbol{\eta}} \le (\frac{\beta_3}{2}) \tilde{\boldsymbol{\nu}}^T \mathbf{H}_3 \tilde{\boldsymbol{\nu}} + (\frac{1}{2\beta_3}) \hat{\boldsymbol{\eta}}^T (\Delta\mathbf{A}_1 + \mathbf{K}_2)^T \mathbf{H}_3^{-1} (\Delta\mathbf{A}_1 + \mathbf{K}_2) \hat{\boldsymbol{\eta}}. \quad (48)$$

Substituting (46)–(48) in (38), adding (38) and (39) yields

$$\begin{aligned}\dot{V} \le& -\tilde{\boldsymbol{\eta}}^T \{\mathbf{K}_1 - (\frac{1}{2\beta_2})(\Delta\mathbf{A}_1 + \mathbf{K}_2)^T \mathbf{H}_2^{-1} (\Delta\mathbf{A}_1 + \mathbf{K}_2)\} \tilde{\boldsymbol{\eta}} \\ & - \tilde{\boldsymbol{\nu}}^T \{\hat{\mathbf{A}}_2 - (\frac{1}{2})(\beta_1 \mathbf{H}_1 + \beta_2 \mathbf{H}_2 + \beta_3 \mathbf{H}_3)\} \tilde{\boldsymbol{\nu}} \\ & - \hat{\boldsymbol{\eta}}^T \{\mathbf{K} - (\frac{1}{2\beta_3})(\Delta\mathbf{A}_1 + \mathbf{K}_2)^T \mathbf{H}_3^{-1} (\Delta\mathbf{A}_1 + \mathbf{K}_2)\} \hat{\boldsymbol{\eta}} \\ & - \hat{\boldsymbol{\nu}}^T \{\rho \mathbf{I} - (\frac{1}{2\beta_1}) \Delta\mathbf{A}_2^T \mathbf{H}_1^{-1} \Delta\mathbf{A}_2\} \hat{\boldsymbol{\nu}} \\ & - \rho_1 \|\hat{\boldsymbol{\nu}}\|^2 + \tilde{\boldsymbol{\eta}}^T (\mathbf{K} + \mathbf{K}_1) \hat{\boldsymbol{\eta}} + \tilde{\boldsymbol{\nu}}^T \Delta\mathbf{d}. \end{aligned} \quad (49)$$

Using the design conditions (27)–(29) we define the following positive definite matrices:

$$\begin{aligned} \mathbf{Q}_1 &\triangleq \{\mathbf{K}_1 - \frac{1}{2\beta_2}(\Delta\mathbf{A}_1 + \mathbf{K}_2)^T \mathbf{H}_2^{-1} (\Delta\mathbf{A}_1 + \mathbf{K}_2)\} \\ \mathbf{Q}_2 &\triangleq \{\hat{\mathbf{A}}_2 - (\frac{1}{2})(\beta_1 \mathbf{H}_1 + \beta_2 \mathbf{H}_2 + \beta_3 \mathbf{H}_3)\} \\ \mathbf{Q}_3 &\triangleq \{\mathbf{K} - \frac{1}{2\beta_3}(\Delta\mathbf{A}_1 + \mathbf{K}_2)^T \mathbf{H}_3^{-1} (\Delta\mathbf{A}_1 + \mathbf{K}_2)\} \\ \mathbf{Q}_4 &\triangleq \{\rho \mathbf{I} - (\frac{1}{2\beta_1}) \Delta\mathbf{A}_2^T \mathbf{H}_1^{-1} \Delta\mathbf{A}_2\}. \end{aligned}$$

From (49) we have

$$\begin{aligned}\dot{V} \le& -\lambda_{\min}(\mathbf{Q}_1) \|\tilde{\boldsymbol{\eta}}\|^2 - \lambda_{\min}(\mathbf{Q}_2) \|\tilde{\boldsymbol{\nu}}\| - \lambda_{\min}(\mathbf{Q}_3) \|\hat{\boldsymbol{\eta}}\|^2 \\ & - \lambda_{\min}(\mathbf{Q}_4) \|\hat{\boldsymbol{\nu}}\|^2 + \|(\mathbf{K} + \mathbf{K}_1)\| \|\tilde{\boldsymbol{\eta}}\| \|\hat{\boldsymbol{\eta}}\| \\ & + \|\tilde{\boldsymbol{\nu}}\| \|\mathbf{d}\| - \rho_1 \|\hat{\boldsymbol{\nu}}\|^2. \end{aligned} \quad (50)$$

From the definition of $\boldsymbol{\xi}$ as in (35) we have $\|\boldsymbol{\xi}\| \ge \|\hat{\boldsymbol{\nu}}\|$, $\|\boldsymbol{\xi}\| \ge \|\tilde{\boldsymbol{\nu}}\|$, $\|\boldsymbol{\xi}\| \ge \|\hat{\boldsymbol{\eta}}\|$, and $\|\boldsymbol{\xi}\| \ge \|\tilde{\boldsymbol{\eta}}\|$. Moreover,

$$\alpha \int_{t-h}^{t} \|(\mathbf{K}_1 + \mathbf{K})\| \|\hat{\boldsymbol{\eta}}(\zeta)\| \|\tilde{\boldsymbol{\eta}}(\zeta)\| \mathrm{d}\zeta \ge \alpha \|(\mathbf{K}_1 + \mathbf{K})\| \|\hat{\boldsymbol{\eta}}(t)\| \|\tilde{\boldsymbol{\eta}}(t)\|, \quad \forall t \ge 0$$

where $\alpha > 1$ by design. Using these conditions, the expression of ρ_1 from (30) and the upper bound of $\mathbf{d}$ from Assumption 1, $\dot{V}$ from (50) yields

$$\dot{V} \le -\varrho_m \|\boldsymbol{\xi}\|^2 + \|\Delta\mathbf{d}\| \|\boldsymbol{\xi}\| - \|(\mathbf{K} + \mathbf{K}_1)\| \|\tilde{\boldsymbol{\eta}}\| \|\hat{\boldsymbol{\eta}}\| (\alpha \|\hat{\boldsymbol{\nu}}\|^2 - 1) \quad (51)$$

where $\varrho_m \triangleq \min_{i=1,2,3,4}\{\lambda_{\min}(\mathbf{Q}_i)\}$.

Consider a scalar $\sigma \in \mathbb{R}^+$ such that $0 < \sigma < \varrho_m$. The definition of V in (35) yields $V \le \|\boldsymbol{\xi}\|^2$. Hence,

$$\begin{aligned}\dot{V} \le& -\varrho_m \|\boldsymbol{\xi}\|^2 + \|\Delta\mathbf{d}\| \|\boldsymbol{\xi}\| \\ & - \|(\mathbf{K} + \mathbf{K}_1)\| \|\tilde{\boldsymbol{\eta}}\| \|\hat{\boldsymbol{\eta}}\| (\alpha \|\hat{\boldsymbol{\nu}}\|^2 - 1) \\ =& -(\varrho_m - \sigma) \|\boldsymbol{\xi}\|^2 - \sigma \|\boldsymbol{\xi}\|^2 + \|\Delta\mathbf{d}\| \|\boldsymbol{\xi}\| \\ & - \|(\mathbf{K} + \mathbf{K}_1)\| \|\tilde{\boldsymbol{\eta}}\| \|\hat{\boldsymbol{\eta}}\| (\alpha \|\hat{\boldsymbol{\nu}}\|^2 - 1) \\ \le& -\sigma V - \|\boldsymbol{\xi}\| \{(\varrho_m - \sigma) \|\boldsymbol{\xi}\| - \|\Delta\mathbf{d}\|\} \\ & - \|(\mathbf{K} + \mathbf{K}_1)\| \|\tilde{\boldsymbol{\eta}}\| \|\hat{\boldsymbol{\eta}}\| (\alpha \|\hat{\boldsymbol{\nu}}\|^2 - 1). \end{aligned} \quad (52)$$

Thus, one has $\dot{V} \le -\sigma V$ when $\alpha \|\hat{\boldsymbol{\nu}}\|^2 \ge 1 \Rightarrow \|\hat{\boldsymbol{\nu}}\| \ge \sqrt{1/\alpha}$ and $(\varrho_m - \sigma) \|\boldsymbol{\xi}\| \ge \|\Delta\mathbf{d}\| \Rightarrow \|\boldsymbol{\xi}\| \ge (\|\Delta\mathbf{d}\| / (\varrho_m - \sigma))$. Since $\|\boldsymbol{\xi}\| \ge \|\hat{\boldsymbol{\nu}}\|$ by definition, the combined condition for $\dot{V} \le -\sigma V$ turns out to be

$$\min\{\|\hat{\boldsymbol{\nu}}\|, \|\boldsymbol{\xi}\|\} \ge \max\{(\|\Delta\mathbf{d}\| / (\varrho_m - \sigma)),\ \sqrt{1/\alpha}\} \Rightarrow \|\hat{\boldsymbol{\nu}}\| \ge \max\{(\|\Delta\mathbf{d}\| / (\varrho_m - \sigma)),\ \sqrt{1/\alpha}\}. \quad (53)$$

This affirms the UUB condition [39] implying $\tilde{\boldsymbol{\eta}}, \tilde{\boldsymbol{\nu}}, \hat{\boldsymbol{\eta}},\ \hat{\boldsymbol{\nu}} \in \mathcal{L}_\infty \Rightarrow \boldsymbol{\eta}, \boldsymbol{\nu} \in \mathcal{L}_\infty$. ■

Boundedness of Various Signals: From the observer-controller co-design (24)–(32), besides boundedness of signals $\boldsymbol{\eta}, \boldsymbol{\nu}, \hat{\boldsymbol{\eta}}, \hat{\boldsymbol{\nu}}$ as proved in the above analysis, boundedness of other closed-loop signals $\rho_1, \boldsymbol{\tau}$, and $\mathbf{K}_2(t)$ can also be proved:

1) $\mathbf{K}_2(t)$ in (31) is always bounded since $\mathbf{J}(t)$ is a bounded orthogonal matrix and $\hat{\mathbf{A}}_1$ is a constant matrix.

2) ρ_1 as in (30) is the result of an integral over a finite time of length h, where h is a user-defined interval (usually the sampling time in practice). Following notion of Reimann integration, $\rho_1(t)$ at any time t is governed by the area covered by the curve $f(\zeta) = (\|(\mathbf{K}_1 + \mathbf{K})\| \|\hat{\boldsymbol{\eta}}(\zeta)\| \|\boldsymbol{\eta}(\zeta) - \hat{\boldsymbol{\eta}}(\zeta)\|)$ and the finite base width h, with ζ spanning from $(t-h)$ to t. Therefore, if $\boldsymbol{\eta}(\zeta)$ and $\hat{\boldsymbol{\eta}}(\zeta)$ are uniformly bounded (i.e., $\boldsymbol{\eta}(\zeta), \hat{\boldsymbol{\eta}}(\zeta) \in \mathcal{L}_\infty$), then $\rho_1(t)$ is also uniformly bounded. With these arguments, one can establish that $\rho_1(t) \in \mathcal{L}_\infty$.

3) From (26) it can be noticed that $\boldsymbol{\tau}$ will be bounded if $\hat{\boldsymbol{\eta}}$, $\hat{\boldsymbol{\nu}}$, ρ_1, and $\mathbf{K}_2$ are bounded. Boundedness of these signals is provided above.

B. Key Performance Indicators

From (53), an ultimate bound on the position error $\boldsymbol{\eta}$ and an upper bound of control input $\boldsymbol{\tau}$ can be computed, which can generate key performance indicators (KPIs) b and $\|\boldsymbol{\tau}\|$.

Let $\iota \triangleq \max\{(\|\Delta\mathbf{d}\| / (\varrho_m - \sigma)),\ \sqrt{1/\alpha}\}$. From (35) we have $V \ge (1/2) \|\hat{\boldsymbol{\nu}}\|^2 \Rightarrow \|\hat{\boldsymbol{\nu}}\| \le \sqrt{2V}$. Thus, from (53), we have $\dot{V} \le -\sigma V$ when

$$\iota \le \|\hat{\boldsymbol{\nu}}\| \le \sqrt{2V} \Rightarrow V \ge \frac{\iota^2}{2}. \quad (54)$$

Therefore, one can deduce the upper bound of V as

$$V \le \max\{V(0),\ \frac{\iota^2}{2}\} \triangleq \mathcal{B}. \quad (55)$$

Utilizing the relations $\|\hat{\boldsymbol{\eta}}\| \le \sqrt{2V}$, $\|\tilde{\boldsymbol{\eta}}\| \le \sqrt{2V}$ and $\|\boldsymbol{\eta}\| = \|\tilde{\boldsymbol{\eta}}\| + \|\hat{\boldsymbol{\eta}}\|$, *the ultimate bound b on the position error $\boldsymbol{\eta}$* can be computed as $b \in [0,\ 2\iota]$. Similarly, *an upper bound on $\boldsymbol{\tau}$* can be derived from (26) as

$$\begin{aligned}\|\boldsymbol{\tau}\| &= \|\mathbf{M}\{\hat{\mathbf{A}}_1 \hat{\boldsymbol{\eta}} + \hat{\mathbf{A}}_2 \hat{\boldsymbol{\nu}} - \mathbf{K}_2 \tilde{\boldsymbol{\eta}} - \mathbf{J}^T \hat{\boldsymbol{\eta}} - (\rho + \rho_1) \hat{\boldsymbol{\nu}}\}\| \\ &\le \sqrt{2\mathcal{B}} \|\mathbf{M}\| \left\{ \|\hat{\mathbf{A}}_1 - \mathbf{J}^T\| + \|\hat{\mathbf{A}}_2 - (\rho + \rho_1)\| + \|\mathbf{K}_2\| \right\}. \end{aligned} \quad (56)$$

Remark 5 (Innovative Aspect of the Proposed Design): The notable feature of the stability result for the proposed DP scheme (24)–(26) is its composite nature: the design jointly provides robustness against model uncertainties, unmodelled thruster dynamics and filtering against measurements. In state-of-the-art DP systems, no composite stability was proposed: either robustness is achieved neglecting filtering (cf. [1], [3], [19]), or filtering is implemented neglecting model uncertainties (cf. [13]–[18]) or neglecting thruster dynamics such as engine dynamics, delay [26].

Remark 6 (Design Guidelines): It can be noticed from (53) and (55) that high values of $\mathbf{K},\mathbf{K}_1,\rho$, and α (determined from (27)–(30)) help to reduce ι and improve control performance. On the other hand, the upper bound (56) reveals that higher values of the above mentioned gains demands higher control effort. Thus, a designer has to make a trade-off between the positioning performance and control effort.

V. Simulation Results and Analysis

In this section, the performance of the proposed controller is validated under the two following scenarios for a heavy lift vessel in "moored" stage (i.e., the heavy load is attached to the platform, and the load is fully/partly on the platform, while the vessel is taking out loading/unloading work trying to transfer the load to/from the vessel from/to the platform):

S1 in the first scenario, the thrusters are considered to be ideal, i.e., no constraint is imposed on its ability of responding to variations in the control input; and

S2 in the second scenario, non-ideal thrusters are considered where low pass filters are used to limit the response to variations in the control input, in line with Section III-C.

Various dynamics parameters of the S-175 ship model used in this work are available as open source in [25]: for convenience, we have summarized them in Appendix. Simulations for both the scenarios are carried out under the "smooth-to-slight" sea-state (i.e., sea state 2) with a current of 0.6 m/s (i.e., 0.3 m/s in north and approximately 0.5 m/s in east). The reason we have chosen sea state 2 is that for most companies, this is the maximum sea state allowed to carry out offshore heavy lift operations [23]. The environmental data under such sea-state are shown in Table II and Fig. 2.

TABLE II
Environment Setting

Current velocity in north and east	Wind velocity	Significant wave height	Mean wind and wave angle
$\begin{bmatrix} u_c \\ v_c \end{bmatrix} = \begin{bmatrix} 0.5 \\ 0.3 \end{bmatrix}$ m/s	2.5 m/s	0.5 m	210°

The thrusters on board consist of three bow thrusters and two propellers. The corresponding thrust allocator matrix is $\mathbf{B}_{ta} = [0.5000; 0.5000; 0-2.67 0.03; 0 2.67 0; 0 1.00 -0.03]$. The nominal value $\hat{\mathbf{A}}_1$ is chosen based on the highest load during the simulation, when $\mathbf{F} = \mathbf{F}_{\max}$, where $\mathbf{F}_{\max}$ refers to the maximum mooring stiffness during the heavy lifting operation, which refers to the mooring stiffness $\mathbf{F}$ with maximum crane load. Thus, $\hat{\mathbf{A}}_1 = 10^{-3}[2.7261\ 0\ 0;\ 0\ 2.0931$

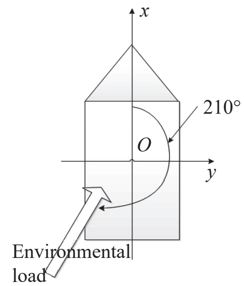

Fig. 2. Environmental load on the vessel.

$-0.0004;\ 0\ -0.0004\ 0.0011]$; nominal value of $\mathbf{A}_2$ is chosen as $\hat{\mathbf{A}}_2 = 10^{-1}[0.1762\ 0\ 0;\ 0\ 1.1312\ -0.6066;\ 0\ -0.0003\ 1.3604]$, which is 90% of the actual value of $\mathbf{A}_2$.

Other parameters involved in the simulation are chosen as: $\mathbf{M} = 10^{10}[0.0026\ 0\ 0;\ 0\ 0.0033\ 0.0015;\ 0\ 0.0015\ 6.5209]$; the upper bound of disturbance is chosen as $\Delta\mathbf{d} = [0.1948,\ 1.4940,\ 0.0012]^T$. The upper bounds of the perturbation $\Delta\mathbf{A}_1$ and $\Delta\mathbf{A}_2$ are selected to be 10% and 100% of $\hat{\mathbf{A}}_1$ and $\hat{\mathbf{A}}_2$, respectively. The various control design parameters are selected as $\alpha = 2$, $\beta_i = 1$, and $\mathbf{H}_i = \Delta\mathbf{A}_2$, $\forall i = 1,2,3$. Consequently, other control gains turn out to be: $\mathbf{K} = \mathbf{K}_1 = 289.78\mathbf{I}$; $\rho = 1.53$. The additional control parameters for S2 are selected as $\bar{N}_i = 300, N_i = 301$, and $h = 0.01$, $\forall i = 1,2,3$.

Throughout the simulation, the tension in the crane wires is considered to follow the pattern depicted in Fig. 3 : such profile emulates the loading and unloading in a crane-vessel system.

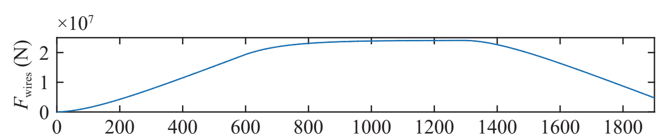

Fig. 3. Tension in the crane wires.

A. Results From Scenario S1

The performance of the proposed controller in this scenario is shown in Figs. 4–6. Its performance is compared with the design in [30], which employs a nonlinear passive observer with a (non-robust) PID controller. The PID controller is tuned for a load of 2460 ton (i.e., approximately 10% mass of the vessel) on the platform under sea state 2, and the parameters are fixed during the whole simulation. The performance of both the proposed and the PID strategy can be checked in the first column of Tables III and IV ($\vartheta = 0$). Both the root mean square error (RMSE) and the maximum offset from the desired equilibrium position are reported. These values show that the proposed approach reduces the RMSE by 89% in north direction, 50% in east direction and 82% in yaw. Offset reductions are 95% in north direction, 78% in east direction, and 83% in yaw.

B. Results From Scenario S2

In this scenario, the thrust allocators are considered to be embedded with the following low pass filters:

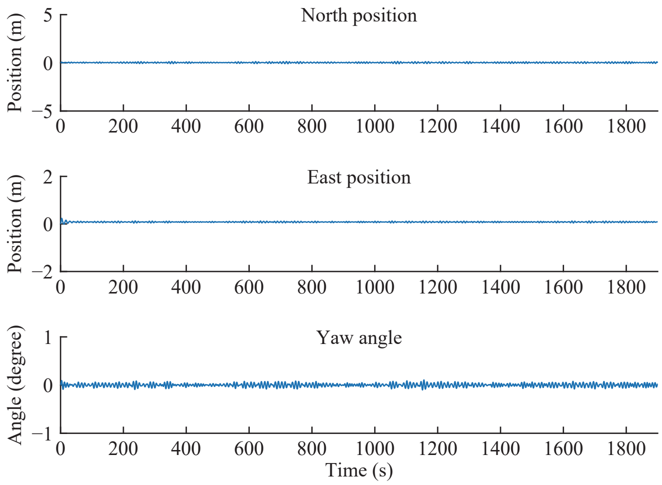

Fig. 4. Vessel position in scenario S1 employing the proposed controller.

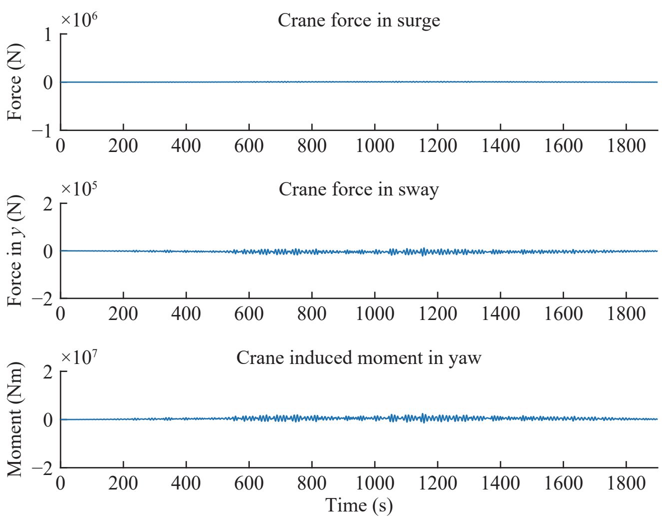

Fig. 5. Crane forces and moment in scenario S1 with the proposed controller.

TABLE III
PERFORMANCE OF THE PROPOSED CONTROLLER WITH THRUSTER DYNAMICS

ϑ		0	1	2	3	4	5
RMSE	North (m)	0.05	0.02	0.03	0.03	0.05	0.07
	East (m)	0.08	0.08	0.08	0.08	0.08	0.09
	Yaw (°)	0.03	0.01	0.02	0.03	0.03	0.03
Maximum offset	North (m)	0.14	0.04	0.06	0.10	0.20	0.24
	East (m)	0.24	0.14	0.19	0.23	0.26	0.31
	Yaw (°)	0.11	0.04	0.08	0.10	0.11	0.09

$$H(s) = \frac{1}{\vartheta s + 1} \tag{57}$$

where ϑ denotes the filter time constant.

The performance of the proposed controller and same PID controller in scenario S1 is verified for five different ϑs as $\vartheta = 1, 2, 3, 4,$ and 5. These values correspond to five possible unmodelled thruster dynamics. The performance of both controllers are tabulated in Tables III and IV, respectively (cf.

TABLE IV
PERFORMANCE OF PID CONTROLLER [30] WITH THRUSTER DYNAMICS

ϑ		0	1	2	3	4	5
RMSE	North (m)	0.44	0.52	0.68	1.32	4.76	12.75
	East (m)	0.16	0.16	0.16	0.17	0.18	0.21
	Yaw (°)	0.17	0.12	0.15	0.13	0.12	0.14
Maximum offset	North (m)	2.61	2.89	3.15	3.87	13.22	43.70
	East (m)	1.11	1.27	1.43	1.54	1.67	1.79
	Yaw (°)	0.63	0.39	0.55	0.50	0.44	0.52

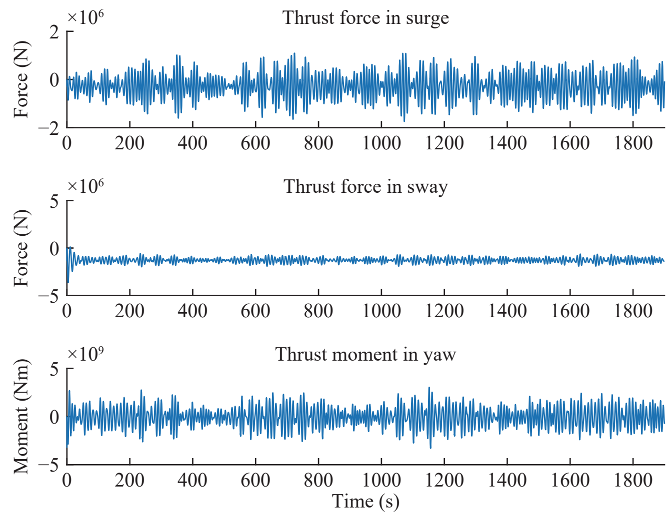

Fig. 6. Thrust forces and moment in S1 with the proposed controller.

the columns corresponding to $\vartheta = 1, 2, 3, 4,$ and 5). Furthermore, for the value $\vartheta = 3$, the results are shown in Figs. 7–9 (proposed controller), and Figs. 10 and 11 (PID controller). The tabulated data reveal that both the proposed controller and the PID controller loose performance as ϑ increases. However, the proposed controller outperforms the PID controller for all ϑ. From the values in the columns $\vartheta = 3$ it is possible to see that the proposed approach reduces the RMSE by 98% in north direction, 53% in east direction and 87% in yaw. Offset reductions are 97% in north direction, 85% in east direction and 80% in yaw. These are similar or larger improvements as compared to $\vartheta = 0$: in other words, the performance of the proposed approach is consistent for a large range of uncertainties.

From Figs. 7 and 8 (proposed controller), and Figs. 10 and 11 (PID controller) it is evident that the PID controller produces large oscillations which are at the onset of instability. Such large oscillations result in forces through the crane wires which are around 10 times larger than the proposed approach.

C. The Role of Propulsion Dynamics and Sea State

A simulation under scenario S2 with $\vartheta = 1$ employing the robust observer [26] in Fig. 12 reveals that propulsion dynamics plays a huge role in determining stability of the DP system. As a matter of fact, state-of-the-art designs can be

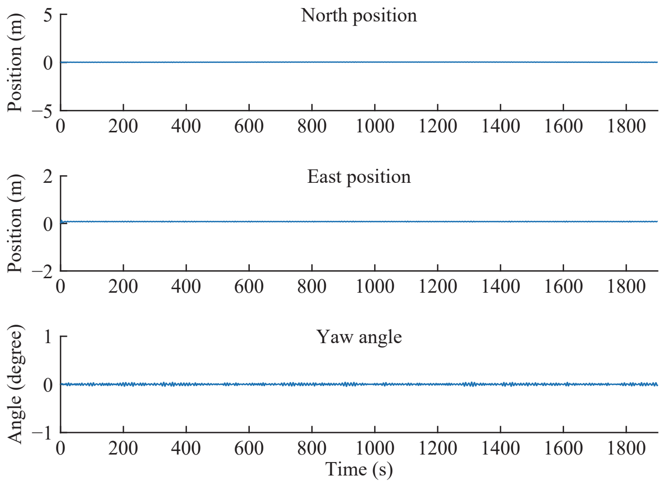

Fig. 7. Vessel position in scenario S2 with the proposed controller, $\vartheta = 3$.

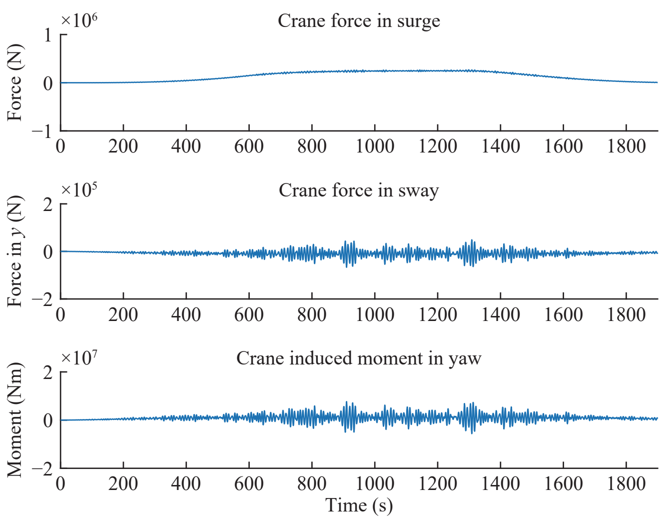

Fig. 8. Crane forces and moment in scenario S2 with the proposed controller, $\vartheta = 3$.

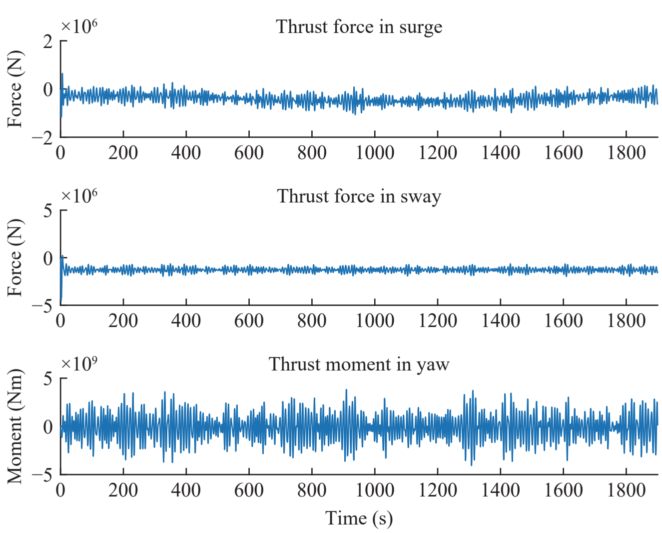

Fig. 9. Thrust forces and moment in S2 with the proposed controller, $\vartheta = 3$.

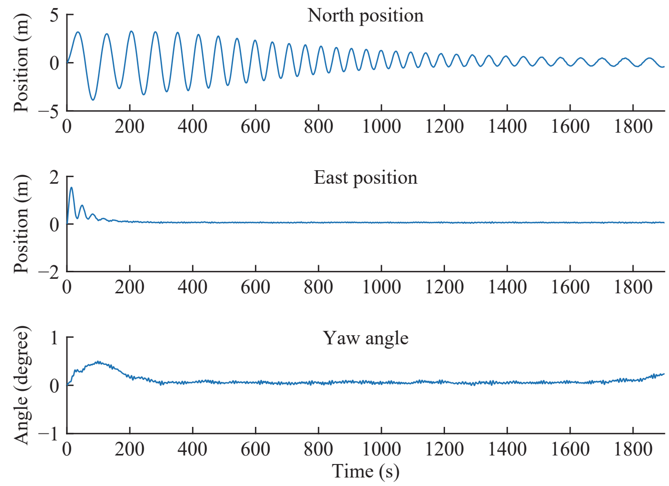

Fig. 10. Vessel position in scenario S2 with PID controller, $\vartheta = 3$.

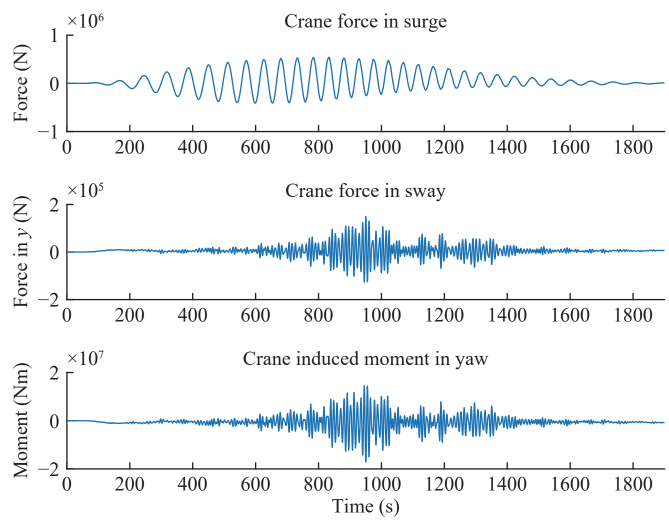

Fig. 11. Crane forces and moment in scenario S2 with PID controller, $\vartheta = 3$.

unstable due to lack of robustness.

More simulations are made with different sea states (Table V), and different loads (Table VI). These results show that the proposed robust controller can still maintain the position of the vessel with a maximum offset of 0.21 m in north, 0.3 m in east, and 0.3° in yaw under sea state 4 (Table V). Moreover, the proposed controller is quite insensitive to different loads, according to Table VI.

VI. Conclusions and Future Work

An observer-based robust DP system was presented for construction crane vessels. The closed-loop control system was proven to be stable under against uncertainty; the effectiveness of the proposed scheme was verified in comparative simulations incorporating real-life uncertain scenarios such as changing mooring force, environmental load, unmodelled propulsion dynamics, and thruster delay. An important future work is embed estimators in the DP control framework to avoid worst-case uncertainty bounds.

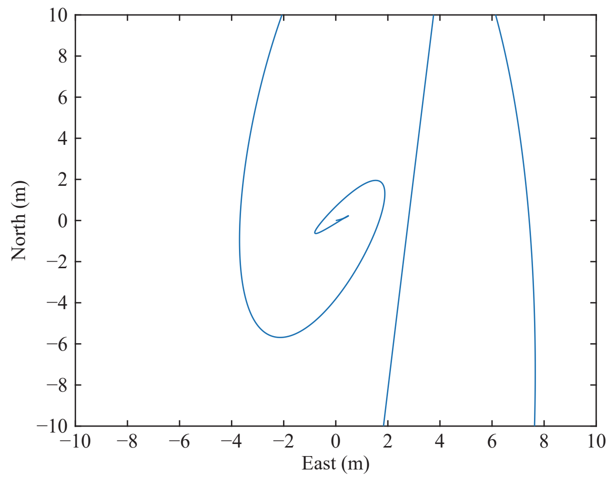

Fig. 12. Unstable behavior with controller from [26], $\vartheta = 3$, due to neglecting propulsion dynamics.

TABLE V
SIMULATION RESULTS OF THE PROPOSED ROBUST CONTROLLER UNDER DIFFERENT SEA STATES, $\vartheta = 3$

Sea state		0	1	2	3	4
RMSE	North (m)	0.01	0.02	0.03	0.05	0.06
	East (m)	0.00	0.03	0.08	0.09	0.09
	Yaw (°)	0.00	0.01	0.02	0.06	0.08
Maximum offset	North (m)	0.01	0.03	0.09	0.15	0.21
	East (m)	0.00	0.07	0.23	0.25	0.30
	Yaw (°)	0.00	0.02	0.09	0.20	0.30

TABLE VI
SIMULATION RESULTS OF THE PROPOSED ROBUST CONTROLLER WITH DIFFERENT LOADS, $\vartheta = 3$

Load (tonnes)		1600	1800	2000	2200	2400
RMSE	North (m)	0.03	0.03	0.03	0.04	0.04
	East (m)	0.08	0.08	0.08	0.08	0.08
	Yaw (°)	0.03	0.02	0.02	0.03	0.02
Maximum offset	North (m)	0.09	0.08	0.06	0.09	0.10
	East (m)	0.21	0.23	0.23	0.24	0.20
	Yaw (°)	0.08	0.08	0.09	0.11	0.08

APPENDIX
NUMERICAL VALUES FOR THE PROCESS PLANT MODEL

The parameters mentioned in Section II are summarized in Table VII, and they are based on the open source S-175 vessel model [25].

TABLE VII
NUMERICAL VALUES FOR THE VARIOUS CRANE VESSEL COMPONENTS

Vessel parameters	
Draught	9.5 m
Breadth	25.4 m
Length between perpendiculars	175 m
Mass (M)	24 609 620 kg
Density of water (ρ_w)	1025 kg/m^3
Acceleration of gravity (g)	9.81 m/s^2
Transverse metacentric height ($\overline{GM}_T$)	0.996 m
Lateral metacentric height ($\overline{GM}_L$)	204.436 m
Block coefficient	0.569
Radius of gyration in roll	8.331 m
Radius of gyration in pitch	42 m
Radius of gyration in yaw	42 m
A_{Fw}	270 m^2
A_{Lw}	2500 m^2
$C_Z = C_K = C_M$	0
A_{wp}	3150 m^2
$\overline{GM}_L$	204.436 m
$\overline{GM}_T$	0.996 m
Engine parameters	
Nominal fuel injection (m_f)	1.3148
Nominal engine efficiency (η_e)	0.38
Nominal engine speed (n_{eng})	1.5 Hz
Nominal engine power	960 kW
Crane wires	
k_w	1.68×10^8 N/m
D_w	4.07×10^5 Ns/m
Hydraulic winch	
η_{hyd}	0.9
K_{hp}	4.0
K_{hi}	0.4
Propeller parameters	
Diameter of the propeller (D_{prop})	3 m
$\{K_{ta}, K_{tb}\}$	$\{-0.438, 0.4773\}$
$\{K_{qa}, K_{qb}\}$	$\{-0.06, 0.7124\}$
Fuel and gearbox parameters	
Lower heating value (k_{LHV})	42 700 kJ/kg
Gearbox ratio (i_{gb})	5.414
Total mass of inertia of propulsion system (I_{tot})	200 kg/m^2
Transmission efficiency (η_{trm})	0.95

$$\mathbf{M}_{RB} = 10^6 \begin{bmatrix} 24.6 & 0 & 0 & 0 & -1.23 & 0 \\ 0 & 24.6 & 0 & 1.23 & 0 & 0 \\ 0 & 0 & 24.6 & 0 & 0 & 0 \\ 0 & 1.2 & 0 & 171 & 0 & 0 \\ -1.23 & 0 & 0 & 0 & 4340 & 0 \\ 0 & 0 & 0 & 0 & 4340 & 0 \end{bmatrix}$$

$$\mathbf{M}_A = 10^6 \begin{bmatrix} 1.40 & 0 & 0 & 0 & 0 & 0 \\ 0 & 11.7 & 0 & -9.95 & 0 & 49.8 \\ 0 & 0 & 30.0 & 0 & 97.0 & 0 \\ 0 & -7.88 & 0 & 235 & 0 & -633 \\ 0 & 0 & 98.1 & 0 & 2920 & 0 \\ 0 & 14.9 & 0 & -444 & 0 & 2890 \end{bmatrix}.$$

Other system parameters are provided in Table VII, which are used to generate the other system dynamics terms such as $\mathbf{C}, \mathbf{D}_s, \mathbf{G}, \mathbf{g}_0$) [29, Section 7.3.1] and propulsion dynamics terms as elaborated in Section II.

References

[1] A. Grovlen and T. I. Fossen, "Nonlinear control of dynamic positioned ships using only position feedback: An observer backstepping approach," in *Proc. 35th IEEE Conf. Decision and Control*, Kobe, Japan, 1996, pp. 3388−3393.

[2] J. M. Godhavn, T. I. Fossen, and S. P. Berge, "Non-linear and adaptive backstepping designs for tracking control of ships," *Int. J Adapt. Control Signal Process.*, vol. 12, no. 8, pp. 649–670, Dec. 1998.

[3] T. I. Fossen and A. Grovlen, "Nonlinear output feedback control of dynamically positioned ships using vectorial observer backstepping," *IEEE Trans. Control Syst. Technol.*, vol. 6, no. 1, pp. 121–128, Jan. 1998.

[4] X. M. Sun and S. S. Ge, "Adaptive neural region tracking control of multi-fully actuated ocean surface vessels," *IEEE/CAA J. Autom. Sinica*, vol. 1, no. 1, pp. 77–83, Jan. 2014.

[5] I. B. Utne, B. Rokseth, A. J. Sørensen, and J. E. Vinnem, "Towards supervisory risk control of autonomous ships," *Reliab. Eng. Syst. Saf.*, vol. 196, pp. 106757, Apr. 2020.

[6] R. H. Rogne, T. H. Bryne, T. I. Fossen, and T. A. Johansen, "On the usage of low-cost mems sensors, strapdown inertial navigation, and nonlinear estimation techniques in dynamic positioning," *IEEE J. Ocean. Eng.*, 2020. DOI: 10.1109/JOE.2020.2967094.

[7] Y. C. Cao and T. S. Li, "Review of antiswing control of shipboard cranes," *IEEE/CAA J. Autom. Sinica*, vol. 7, no. 2, pp. 346–354, Mar. 2020.

[8] J. Flint and R. Stephens, "Dynamic positioning for heavy lift applications," in *Proc. Annu. Conf. Dynamic Positioning Conf.*, Houston, Texas, USA, 2008, pp. 200−233.

[9] J. Ye, M. Godjevac, and E. el Amam, "Position control of crane vessel during offshore installations: Using adaptive and robust control methods," in *Proc. 21st Int. Conf. System Theory, Control and Computing*, Sinaia, Romania, 2017, pp. 17−22.

[10] S. Messineo and A. Serrani, "Offshore crane control based on adaptive external models," *Automatica*, vol. 45, no. 11, pp. 2546–2556, Nov. 2009.

[11] B. V. E. How, S. S. Ge, and Y. S. Choo, "Dynamic load positioning for subsea installation via adaptive neural control," *IEEE J. Ocean. Eng.*, vol. 35, no. 2, pp. 366–375, Apr. 2010.

[12] J. F. Yu, Q. S. Li, and W. J. Zhou, "Nonlinear robust stabilization of ship roll by convex optimization," *IEEE/CAA J. Autom. Sinica*, 2016. DOI: 10.1109/JAS.2016.7510163

[13] J. L. Du, Y. Yang, D. H. Wang, and C. Guo, "A robust adaptive neural networks controller for maritime dynamic positioning system," *Neurocomputing*, vol. 110, pp. 128–136, Jun. 2013.

[14] J. L. Du, X. Hu, M. Krstić, and Y. Q. Sun, "Dynamic positioning of ships with unknown parameters and disturbances," *Control Eng. Pract.*, vol. 76, pp. 22–30, Jul. 2018.

[15] X. Hu and J. L. Du, "Robust nonlinear control design for dynamic positioning of marine vessels with thruster system dynamics," *Nonlinear Dyn.*, vol. 94, pp. 365–376, Oct. 2018.

[16] Y. H. Wang, Y. L. Tuo, S. X. Yang, M. Biglarbegian, and M. Y. Fu, "Reliability-based robust dynamic positioning for a turret-moored floating production storage and offloading vessel with unknown time-varying disturbances and input saturation," *ISA Trans.*, vol. 78, pp. 66–79, Jul. 2018.

[17] Z. J. Sun, G. Q. Zhang, L. Qiao, and W. D. Zhang, "Robust adaptive trajectory tracking control of underactuated surface vessel in fields of marine practice," *J. Mar. Sci. Technol.*, vol. 23, no. 4, pp. 950–957, Dec. 2018.

[18] W. Z. Yu, H. X. Xu, and H. Feng, "Robust adaptive fault-tolerant control of dynamic positioning vessel with position reference system faults using backstepping design," *Int. J. Robust Nonlinear Control*, vol. 28, no. 2, pp. 403–415, Jan. 2018.

[19] A. H. Brodtkorb, S. A. Værnø, A. R. Teel, A. J. Sørensen, and R. Skjetne, "Hybrid controller concept for dynamic positioning of marine vessels with experimental results," *Automatica*, vol. 93, pp. 489–497, Jul. 2018.

[20] K. D. Do, "Global robust and adaptive output feedback dynamic positioning of surface ships," in *Proc. IEEE Int. Conf. Robotics and Automation*, Roma, Italy, 2007, pp. 4271−4276.

[21] M. Y. Fu, L. L. Yu, M. Y. Li, Y. L. Tuo, and C. L. Ni, "Synchronization control of multiple surface vessels without velocity measurements," in *Proc. IEEE Int. Conf. Mechatronics and Automation*, Beijing, China, 2015, pp. 643−648.

[22] Z. H. Peng, L. Liu, and J. Wang, "Output-feedback flocking control of multiple autonomous surface vehicles based on data-driven adaptive extended state observers," *IEEE Trans. Cybern.*, 2020. DOI: 10.1109/TCYB.2020.3009992.

[23] F. C. Bakker, "A conceptual solution to instable dynamic positioning during offshore heavy lift operations using computer simulation techniques," M.S. thesis, Delft University of Technology, The Netherlands, 2015.

[24] Y. G. Sun, H. Y. Qiang, J. Q. Xu, and D. S. Dong, "The nonlinear dynamics and anti-sway tracking control for offshore container crane on a mobile harbor," *J. Mar. Sci. Technol.*, vol. 25, no. 6, pp. 656–665, Nov. 2017.

[25] T. I. Fossen and T. Perez, "Marine systems simulator (MSS)," https://github.com/cybergalactic/MSS, accessed 2004.

[26] J. Ye, S. Roy, M. Godjevac, and S. Baldi, "Observer-based robust control for dynamic positioning of large-scale heavy lift vessels," *IFAC-PapersOnLine*, vol. 52, no. 3, pp. 138–143, Jan. 2019.

[27] P. A. Ioannou and J. Sun, *Robust Adaptive Control*. Upper Saddle River, NJ: Prentice-Hall, 1996.

[28] A. J. Sørensen, "Structural issues in the design and operation of marine control systems," *Annu. Rev. Control*, vol. 29, no. 1, pp. 125–149, Dec. 2005.

[29] T. I. Fossen, *Handbook of Marine Craft Hydrodynamics and Motion Control*. United Kingdom: John Wiley & Sons, 2011.

[30] J. Ye, M. Godjevac, S. Baldi, and H. Hopman, "Joint estimation of vessel position and mooring stiffness during offshore crane operations," *Autom. Construct.*, vol. 101, pp. 218–226, May 2019.

[31] E. F. Brater and H. W. King, *Handbook of Hydraulics for the Solution of Hydraulic Engineering Problems*. New York: McGraw-Hill, 1976.

[32] G. C. Goodwin, S. F. Graebe, and M. E. Salgado, *Control System Design*. Upper Saddle River, NJ: Prentice Hall, 2001.

[33] M. Godjevac and M. Drijver, "Performance evaluation of an inland pusher," in *Transport of Water versus Transport over Water*, C. Ocampo-Martinez and R. Negenborn, Eds. Switzerland: Springer, 2015, pp. 389−411.

[34] R. D. Geertsma, R. R. Negenborn, K. Visser, M. A. Loonstijn, and J. J. Hopman, "Pitch control for ships with diesel mechanical and hybrid propulsion: Modelling, validation and performance quantification," *Appl. Energy*, vol. 206, pp. 1609–1631, Nov. 2017.

[35] S. Roy, J. Lee, and S. Baldi, "A new adaptive-robust design for time delay control under state-dependent stability condition," *IEEE Trans. Control Syst. Technol.*, vol. 29, no. 1, pp. 420–427, Jan. 2021.

[36] T. I. Fossen and J. P. Strand, "Passive nonlinear observer design for ships using Lyapunov methods: Full-scale experiments with a supply vessel," *Automatica*, vol. 35, no. 1, pp. 3–16, Jan. 1999.

[37] S. Ogutcu, "Assessing the contribution of galileo to GPS+GLONASS

PPP: Towards full operational capability," *Measurement* , vol. 151, pp. 107143, Feb. 2020.

[38] J. E. Bremnes, A. H. Brodtkorb, and A. J. Sørensen, "Sensor-based hybrid translational observer for underwater navigation," *IFAC-PapersOnLine*, vol. 52, no. 21, pp. 378–383, Jan. 2019.

[39] H. K. Khalil, *Nonlinear Systems*. 3rd ed. Upper Saddle River, NJ: Prentice Hall, 2002.

[40] T. Tao, S. Roy, and S. Baldi, "The issue of transients in leakage-based model reference adaptive control of switched linear systems," *Nonlinear Anal.*: *Hybrid Syst.*, vol. 36, pp. 100885, May 2020.

[41] S. Roy, I. N. Kar, J. Lee, N. G. Tsagarakis, and D. G. Caldwell, "Adaptive-robust control of a class of EL systems with parametric variations using artificially delayed input and position feedback," *IEEE Trans. Control Syst. Technol.*, vol. 27, no. 2, pp. 603–615, Mar. 2019.

Jun Ye received the B.Sc. in marine engineering at Shanghai Jiao Tong University in China (2009–2013), and the M.Sc. in marine engineering at Delft University of Technology, The Netherlands (2014–2016). She recently received the Ph.D. in maritime and transport technology from Delft University of Technology in 2020. Her research focuses on modelling, dynamic positioning, and autonomy of heavy lift vessels.

Spandan Roy received the B.Tech degree in electronics and communication engineering from Techno India (Salt Lake), West Bengal University of Technology, India in 2011, the M.Tech. degree in mechatronics from Academy of Scientific and Innovative Research (AcSIR), India in 2013 and Ph.D. degree in control and automation from Indian Institute of Technology Delhi (IITD), India in 2018. He is currently Assistant Professor with Robotics Research Center, International Institute of Information Technology Hyderabad, India. Previously, he was Postdoc with Delft Center for System and Control, TU Delft, The Netherlands. He is Subject Editor of *Int. Journal of Adaptive Control and Signal Processing*. His research interests include artificial delay based control, adaptive-robust control, switched systems and its applications in Euler–Lagrange systems.

Milinko Godjevac works as a Senior R&D Engineer at Future Proof Shipping and previously at Allseas Engineering b.v. His field of expertise is system integration of dynamic positioning and ship propulsion systems. He graduated in Naval Architecture at Belgrade University and obtained the Ph.D. title in marine engineering from Delft University of Technology.

Vasso Reppa (M' 06) has been an Assistant Professor in the Department of Maritime and Transport Technology, Delft University of Technology since 2018. She obtained the doctorate (2010) in electrical and computer engineering from the University of Patras, Greece. From 2011 to 2017, she was a Research Associate (now Research Affiliate) with the KIOS Research and Innovation Center of Excellence in Cyprus. In 2013, Dr. Reppa was awarded the Marie Curie Intra European Fellowship and worked as a Research Fellow in CentraleSupélec of the University Paris-Saclay, France from 2014 to 2016. She was a Visiting Researcher at Imperial College, the UK and at University of Newcastle, Australia in 2015 and 2016, respectively. Her research interests include distributed fault diagnosis and fault tolerant control, adaptive learning, observer-based estimation, and applications of autonomous systems in transport, smart buildings, and robotics.

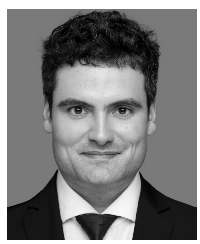

Simone Baldi (M'14–SM'19) received the B.Sc. in electrical engineering, and the M.Sc. and Ph.D. in automatic control engineering from University of Florence, Italy, in 2005, 2007, and 2011, respectively. He is Professor at School of Mathematics and School of Cyber Science and Engineering, Southeast University, with guest position at Delft Center for Systems and Control, TU Delft, where he was Assistant Professor. He was awarded Outstanding Reviewer for *Automatica* (2017). He is Subject Editor of *Int. Journal of Adaptive Control and Signal Processing* and Associate Editor of *IEEE Control Systems Letters*. His research interests are adaptive and learning systems with applications in unmanned vehicle systems.